LASER-INDUCED BIOACTIVITY IN DENTAL PORCELAIN MODIFIED BY BIOACTIVE GLASS

ANASTASIA BEKETOVA, MARIANTHI MANDA, DEMETRIOS CHAROULIS, DIMITRIS CHRISTOFILOS*, LAMBRINI PAPADOPOULOU**, OURANIA-MENTI GOUDOURI***, EFSTATHIOS POLYCHRONIADIS***, KONSTANTINOS M. PARASKEVOPOULOS***, #PETROS KOIDIS

Department of Fixed Prosthesis and Implant Prosthodontics, Dentistry School, Aristotle University of Thessaloniki, University Campus, Dentistry Building, GR 54124, Thessaloniki, Greece
**Physics Division, School of Technology, Aristotle University of Thessaloniki, University Campus, GR 54124, Thessaloniki, Greece*
***School of Geology, Aristotle University of Thessaloniki, University Campus, GR 54124, Thessaloniki, Greece*
****Physics Department, Aristotle University of Thessaloniki, University Campus, GR 54124, Thessaloniki, Greece*

#E-mail: pkoidis@dent.auth.gr

Submitted February 21, 2012; accepted October 21, 2012

Keywords: Laser-liquid-solid interaction, Bioactive glass, Ceramics, Nano-hydroxyapatite, Bioactivity

The aim of this study was to investigate the impact of laser-liquid-solid interaction method in the bioactivity of dental porcelain modified by bioactive glass. Forty sol-gel derived specimens were immersed in Dulbecco's Modified Eagle's Medium, 31 and 9 specimens of which were treated with Er:YAG and Nd:YAG laser respectively. Untreated specimens served as controls. Incubation of specimens followed. Bioactivity was evaluated, using Fourier Transform Infrared spectroscopy (FTIR), Scanning Electron Microscopy (SEM)/Energy Dispersive Spectroscopy (EDS) and Transmission Electron Microscopy (TEM). FTIR detected peaks associated with hydroxyapatite on 1 Nd:YAG- and 4 Er:YAG-treated specimens. SEM analysis revealed that Er:YAG-treated specimens were covered by granular hydroxyapatite layer, while Nd:YAG treated specimen presented growth of flake-like hydroxyapatite. TEM confirmed the results. The untreated controls presented delayed bioactivity. In conclusion, Nd:YAG and Er:YAG laser treatment of the material, under certain fluencies, accelerates hydroxyapatite formation. Nd:YAG laser treatment of specific parameters causes the precipitation of flake-like hydroxyapatite in nano-scale.

INTRODUCTION

The modification of the sol-gel derived dental porcelain by bioactive glass has been reported to result in an improved composite as far as the bioactive behaviour is concerned, compared to other composite materials of the same oxide system [1-3]. However, further modifications are required in order to achieve the objective of applying in the clinical reality. Despite the fact that the optimization of bioactive behaviour has been achieved mainly by surface processing using chemical synthesis methods, recent research attempts to modify surface's structure by directing the spatial and temporal distribution of laser energy in a liquid precursor solution. The intensity of the laser and the nanosecond time scales result in the development of non-equilibrium conditions (instantaneous extreme temperatures and pressures) at the laser-liquid-solid (substrate) interface, which create the critical thermodynamic driving forces and reaction kinetics of crystal nucleation and growth in the nano-scale [4, 5]. In particular, the laser-induced precipitation of nano-hydroxyapatite crystals on the surface of silicon substrates and silica glass within 24 hours after soaking in simulated body fluid has been already reported in the literature [6]. In this way, it appears possible to control the ability of the material to form nano-hydroxyapatite film in a short period of time, by exploiting the archives of laser technology. Thus, the purpose of the present study was to investigate the impact of the laser-liquid solid interaction (LLSI) in the bioactivity of the sol-gel derived dental porcelain modified by bioactive glass.

EXPERIMENTAL

Materials and methods

The dental porcelain-bioactive glass composite was prepared by the sol-gel method. Accordingly, the precursors of bioactive glass 58S formed the initial solution and during their gelation, dental porcelain powder, used for margin restoration of fixed partial dentures (IPS Inline-Margin Ceramic System, Ivoclar, Schaan, Liechtenstein), was added in the ratio of 50 wt. % [7]. The final mixture was pulverized and a 20 - 40 μm-grained powder was obtained. The powder was mixed with the modelling liquid of dental porcelain and 44 disc specimens

(4.5 × 1.5 mm) were fabricated. The specimens were fired to 930°C, with a rate of 60°C/min in vacuum, according to manufacturers' instructions for dental porcelain. The specimens were marked by a scratch line, dividing them into 2 equal parts. The assessment of *in vitro* bioactivity was carried out by immersing the disk BP specimens in an open glass container, filled with serum-free Dulbecco's Modified Eagle's Medium (DMEM) GIBCO, (Invitrogen Corporation, UK), while, at the same time, laser energy was applied to the marked half of each sample. The other half was left untreated, serving as control. Thirty one specimens were treated using Er:YAG (λ = 2940 nm) and 9 specimens were treated using Nd:YAG (λ = 1064 nm) (Fidelis Plus III, Fotona, Slovenia). The pulsed laser beam was focused in a perpendicular direction on the BP sample-DMEM interface. The samples surface was scanned with different speed depending on the parameters of the laser beam (Table 1 and 2). The level of DMEM above the sample was kept at 2 mm, during the whole process. Immediately after laser treatment, both Nd:YAG (LN)- and Er:YAG (L)-treated specimens were re-immersed in DMEM and incubated at 37 ± 1°C for 6 and 3 days, respectively, while untreated BP control (BPunc) specimens were incubated in DMEM for 30 days. DMEM was renewed every 2nd day. After the removal, the specimens were rinsed with ethanol and distilled water, dried and stored in an airtight container. Bioactivity evaluation was performed by detecting hydroxyapatite layer on the specimens' surface, using: a. extended Fourier Transform Infrared (FTIR) Spectrometer (IFS113v, Bruker) in the mid-infrared region (5000 - 400 cm^{-1}), b. Scanning Electron Microscope (SEM) (JEOL Scanning Microscope JSM 840-A) coupled with Energy Dispersive Spectroscopy (EDS) and c. conventional Transmission Electron Microscopy (TEM) (JEOL 100CX TEM), working in 100 kV.

Table 1. Nd:YAG Laser parameters and sample names (ALP: Average Laser Power, F: Frequency, T: time, PDT: Pulse Duration Time).

		Laser Nd:YAG		
		LN1		
Samples		LN1a	LN2a	LN3a
Laser Parameters	ALP (W)		15	
	F (Hz)		15	
	T (sec)		30	
	PDT (μsec)	100	180	100
		Laser Nd:YAG		
		LN2		
Samples		LN1b	LN2b	LN3b
Laser Parameters	ALP (W)		10	
	F (Hz)		50	
	T (sec)		30	
	PDT (μsec)	100	180	100
		Laser Nd:YAG		
		LN3		
Samples		LN1c	LN2c	LN3c
Laser Parameters	ALP (W)		0.5	
	F (Hz)		10	
	T (sec)		30	
	PDT (μsec)	100	180	100

Table 2. Er:YAG Laser parameters and sample names (ALP: Average Laser Power, F: Frequency, T: time, PDT: Pulse Duration Time).

		Laser Er:YAG					
		L1					
	Samples	L1a	L1b	L1c	L1d	L1e	L1f
Laser Parameters	ALP (W)	1000	600	450	300	150	40
	F (Hz)	12	15	15	15	12	12
	T (sec)	15	15	15	18	31	60
	PDT (μsec)	100					
		Laser Er:YAG					
		L2					
	Samples	L2a	L2b	L2c	L2d	L2e	L2f
Laser Parameters	ALP (W)	1000	600	450	300	150	40
	F (Hz)	12	15	15	15	12	12
	T (sec)	15	15	24	15	25	90
	PDT (μsec)	600					
		Laser Er:YAG					
		L3					
	Samples	L3a	L3b	L3c	L3d	L3e	L3f
Laser Parameters	ALP (W)	1000	600	450	300	150	40
	F (Hz)	12	15	15	15	12	12
	T (sec)	11	10	16	10	23	90
	PDT (μsec)	300					
		Laser Er:YAG					
		L4					
	Samples	L4a	L4b	L4c	L4d	L4e	L4f
Laser Parameters	ALP (W)	700	600	450	300	150	40
	F (Hz)	12	15	15	15	12	12
	T (sec)	9	9	9	13	18	47
	PDT (μsec)	100					
		Laser Er:YAG					
		L5					
	Samples	L5a	L5b	L5c	L5d	L5e	L5f
Laser Parameters	ALP (W)	300	400	450	300	150	80
	F (Hz)	30	20	15	15	12	6
	T (sec)	5	7	8	9	12	38
	PDT (μsec)	50					
		Laser Er:YAG					
	Samples	L6					
Laser Parameters	ALP (W)	1000					
	F (Hz)	20					
	T (sec)	5					
	PDT (μsec)	1000					

RESULTS

FTIR Analysis

Figure 1 displays the FTIR spactra of the BPunc specimens after 12 and 30 days of immersion in DMEM solution, along with the spectra of the LN and L specimens after 3 and 6 days of immersion respectively. Remarkable changes in the reflectance spectra, indicating the *formation* of *hydroxyapatite,* appeared for the: a. L1b, L1e, L4d and L4f specimens after 6 days of immersion, b. LN3b specimen after 3 days of immersion and c. BPunc specimen after 12 and 30 days of immersion in DMEM solution. More specific, all the aforementioned specimens presented an enhancement of the peaks, located at 560 and 602 cm^{-1}, in comparison to the BP as-prepared specimen, which are typical of hydroxyapatite-like phases and are associated with the ν_4 bending mode of PO_4^3 (patterned rectangular in Figure 1) [8]. Furthermore, the L1b, L1e, L4d and L4f specimens, in the 6th post-immersion day, clearly exhibited 4 peaks, associated with the phosphate groups, at: a) 963 cm^{-1}, reflecting the ν_1 P–O symmetric stretch and b) 1030, 1050 and 1096 cm^{-1}, which have been related to the ν_3 P–O antisymmetric stretching vibration (dashed lines in Figure 1) [9].

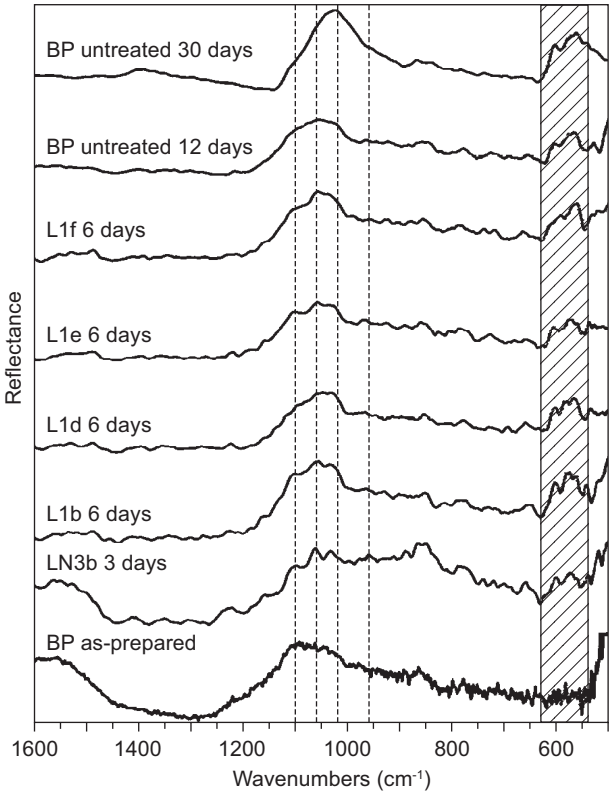

Figure 1. FTIR reflectance spectra of the BPc specimen before immersion in DMEM solution and LN3b, L1b, L1e, L4d, L4f and BPunc specimens after immersion in DMEM solution.

SEM/EDS Analysis

In Figure 2, 3 and 4, the SEM images of the BPunc, the LN3b and the L1b, L1e, L4d, L4f specimens at the end of their immersion time are presented, while Ca–P ratio values of selected spectra, derived from EDS analyses on their surfaces, are shown in Table 3. The surfaces of the BPunc specimen after 12 and 30 days of immersion as well as both the treated and untreated half parts of the L1b, L1e, L4d and L4f were covered by a rough granular layer, with Ca-P ratio varying between 1.42-1.84, corresponding to Ca-deficient hydroxyapatite, as shown by EDS analyses in Table 3. However, the morphology of the hydroxyapatite layer is assigned to the initial stages of hydroxyapatite formation, as opposed to the hydroxyapatite layer developed on the surface of BPunc specimen after 30 days of immersion, which showed high density and deep cracks, typical features of hydroxyapatite with high crystallinity. On the other hand, in the applied range of fluencies, the LN3b specimen exhibited no hydroxyapatite formation on its laser untreated half part, while the laser treated one showed hydroxyapatite growth with flake-like morphology and Ca-P ratio varying between 1.25 - 1.4 (Table 3).

Table 3. EDS analysis on the surface of the: a) BPunc specimens after 12 and 30 days, b) LN3b after 3 days and c) L1b, L1e, L4d and L4f after 6 days of immersion in DMEM solution.

Analysis		Weight % - EDS			
Ratio		Ca–P			
Spectra		1	2	3	4
Specimens	BPunc 12	1.56	1.62	–	–
	BPunc 30	1..65	1.69	–	–
	LN3b	1.40	1.25	1.39	1.36
	L1b	1.75	1.51	1.84	–
	L1e	1.80	1.47	1.61	–
	L4d	1.42	1.58	1.49	–
	L4f	1.56	1.70	1.80	–

TEM analysis

In Figure 5, TEM image of the laser treated half part of the LN3b is presented. TEM analysis showed a flake-like grain lying on the surface of the sample with dimensions approximately 0.7 × 0.16 μm (Figure 5a and b). It was obvious that the dark field image was necessary in order for the grains to be visible as well as to identify its phase by electron diffraction (Figure 5b). The diffraction pattern (Figure 5c) consisted of two different kinds of spots belonging to the same phase. The first kind had individual spots coming from the observed grain and the second one constituted of very fine ones forming a complete ring. Complete circle of spots indicated that the grain size was in nano scale, while both kinds of spot belonged to hydroxyapatite phase, as Table 4 indicated [10].

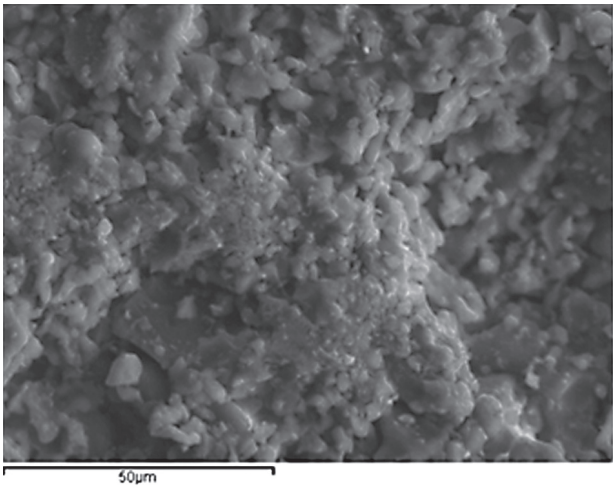

a) 12 days

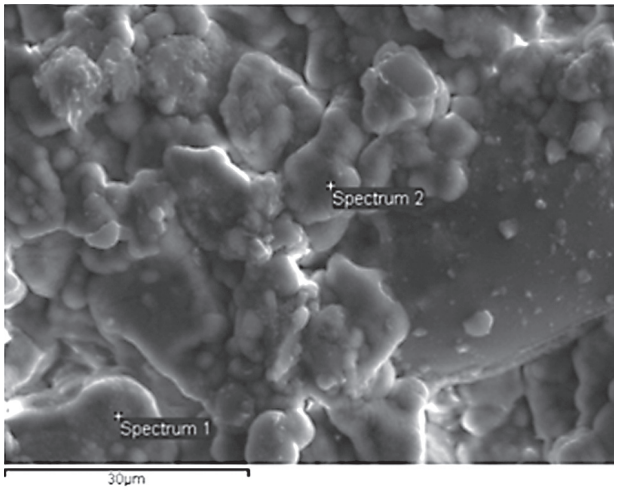

b) 12 days

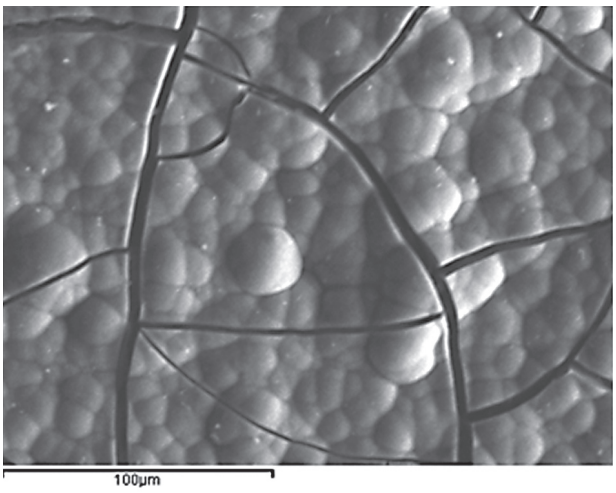

c) 30 days

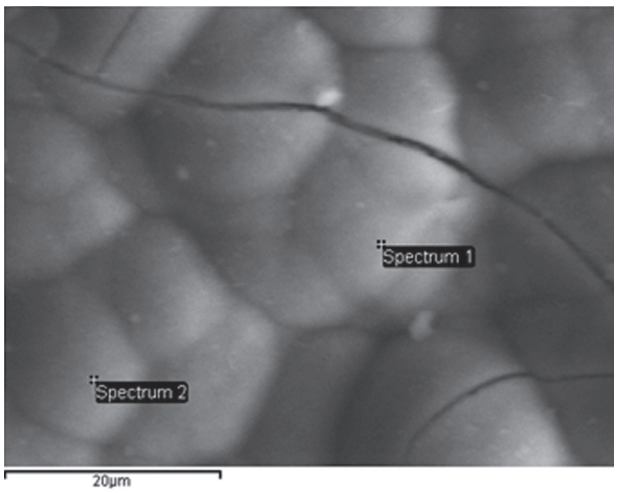

d) 30 days

Figure 2. SEM images of BPunc specimens after 12 (a, b) and 30 days (c, d) of immersion in DMEM solution.

Table 4. Experimental and theoretical d-value (interplanar spacing) of the phase which was identified as hydroxyapatite.

d experimental	d experimental	d theoretical	hkl
7.5	4.06	4.07	200
10.7	2.85	2.814	211
16.6	1.84	1.841	213
15	2.03	2.065	113
14.4	2.163	2.146	311
15.6	1.955	1.943	222
12.2	2.50	2.528	301
13.9	2.194	2.146	311
14.7	2.079	2.065	113

DISCUSSION

The pulsed laser irradiation of different types of solid substrates has been utilized for the rapid synthesis of crystals in the form of nano-films onto their surface, by exploiting the soluble precursors in liquid media and the highly non-equilibrium state occurred in the solid-liquid interface [11, 12]. The aforementioned archives of the, as known, LLSI method have been applied on bioactive materials, which required prolonged period of immersion time in simulated body fluids, in order to develop bioactive behavior. The LLSI method allowed the acceleration and enhancement of crystal nucleation and growth hydroxyapatite nano-film onto their surface [13-15]. Regarding the present study, sol-gel derived dental porcelain modified by bioactive glass 58S was used as a solid target of LLSI method in DMEM solution, which has been characterized as a highly amorphous glass-ceramic composite, being dispersed with leucite, hydroxyapatite-like and wollastonite crystal phases [16]. However, the microstructure as well as the chemical composition in terms of both the percentage and type of the surface crystallization defined from the material's processing parameters, resulted in a material with low bioactivity index [17]. Research studies, reporting on the bioactive behavior of the same material, using conventional *in vitro* tests by soaking it in simulated body

fluids, have concluded that the onset of hydroxyapatite formation occurs after 15 days, considering the material as a non-bioactive [16]. These results are in keeping with the data derived from the present study, which shows that the control composite specimens, without being treated with laser, formed Ca-deficient carbonate hydroxyapatite layer onto their surfaces after 12 days of immersion in DMEM solution. The deposited layer presented the typical characteristics of hydroxyapatite reported in the literature, exhibiting granular and dense morphology, with deep cracks. Taking into account the prolonged time of bioactivity induction along with the characteristic features of the hydroxyapatite layer observed on the untreated control specimens, this study reveals the impact of laser energy application on the hydroxyapatite formation. Specifically, the use of the solid state Nd:YAG laser, which exhibits low optical absorption coefficient of water at the wavelength 1064 nm [18], not only reduced the carbonate hydroxyapatite precipitation time, but also resulted in a deposited hydroxyapatite film with characteristics quite different compared to the typical ones. In particular, Nd:YAG laser, under certain range

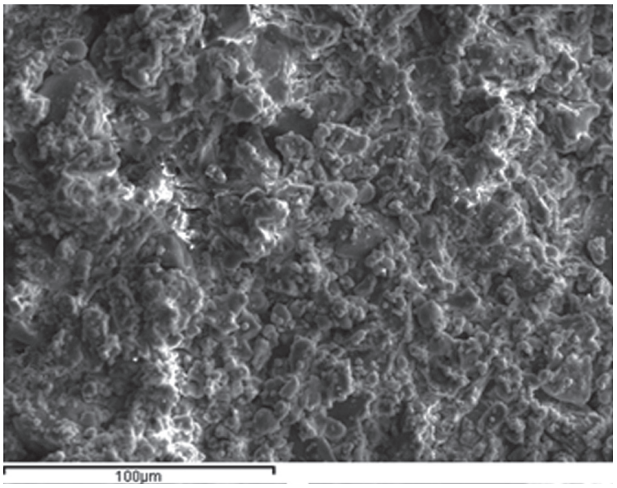

a) LN3b, the laser treated part ×500

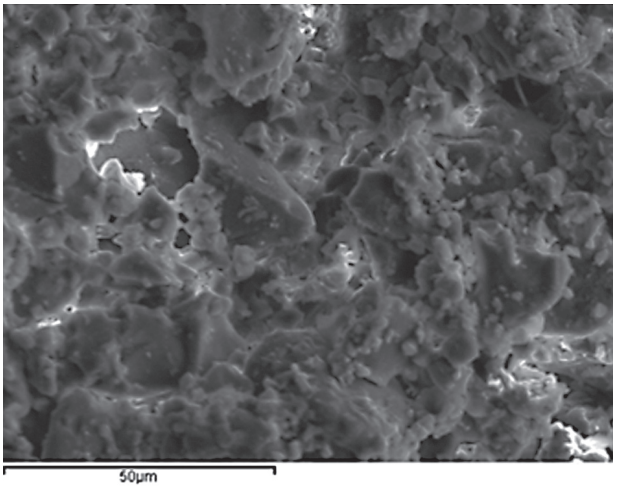

b) LN3b, the untreated part ×1000

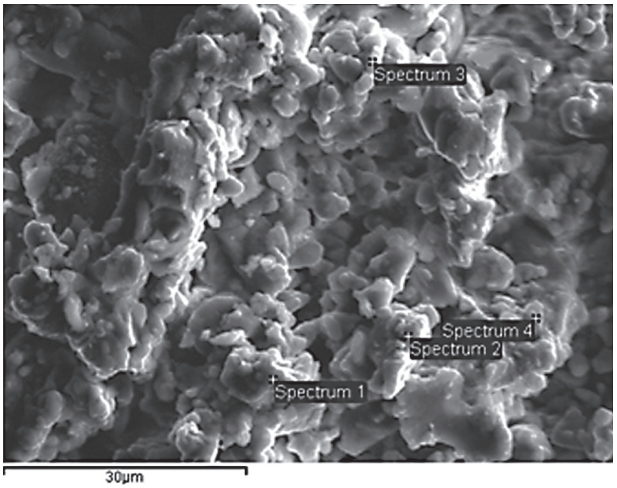

c) LN3b, the laser treated part ×2000

Figure 3. SEM images of the LN3b specimen after 3 days of immersion in DMEM solution: a) the laser treated part ×500, b) the untreated part ×1000 and c) the laser treated part ×2000.

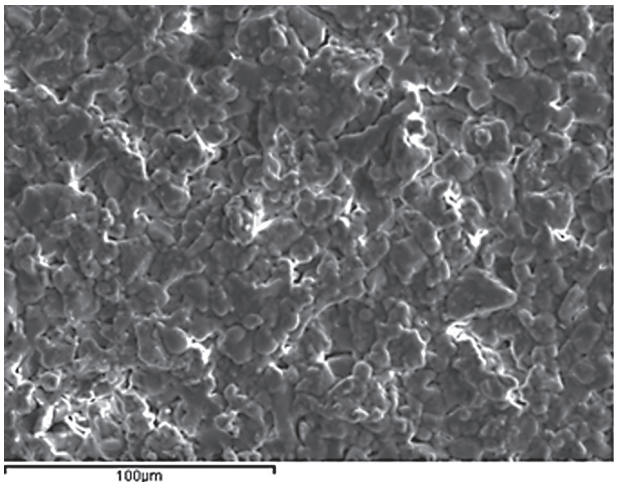

a) L1b (×500)

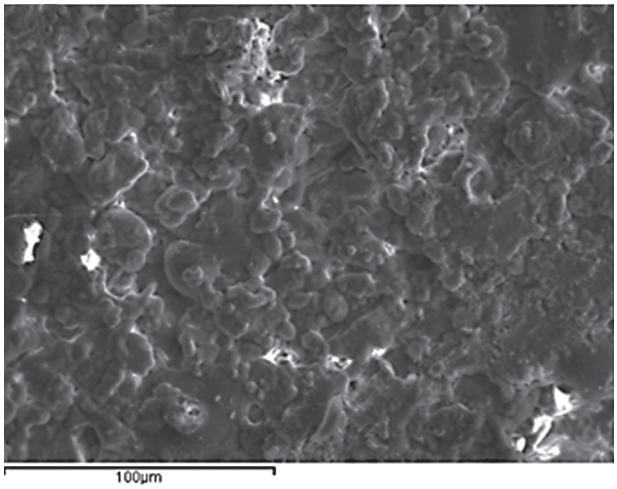

b) L1b (×2000)

Figure 4. SEM images of the laser treated part of the L1b (a, b) specimens after 6 days of immersion in DMEM solution. Magnification ×500 (a) and ×2000 (b). *Continue on next page*

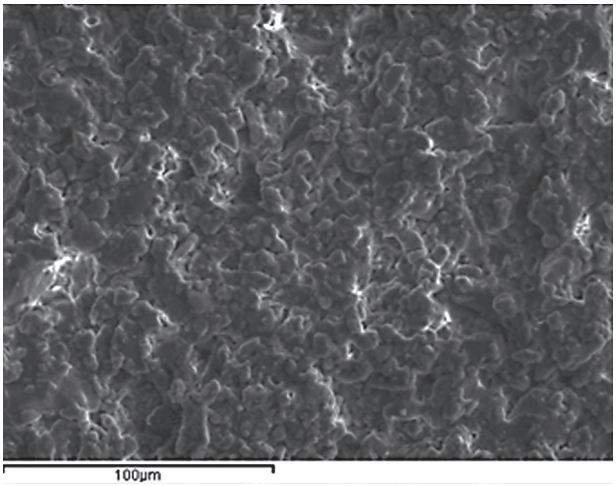

c) L1e (×500)

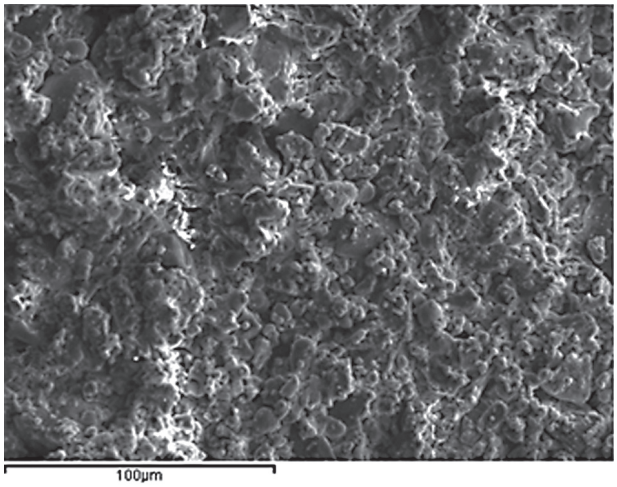

d) L1e (×2000)

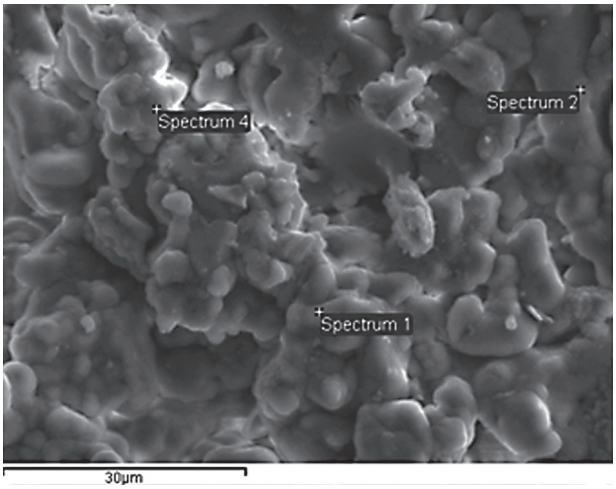

e) L4d (×500)

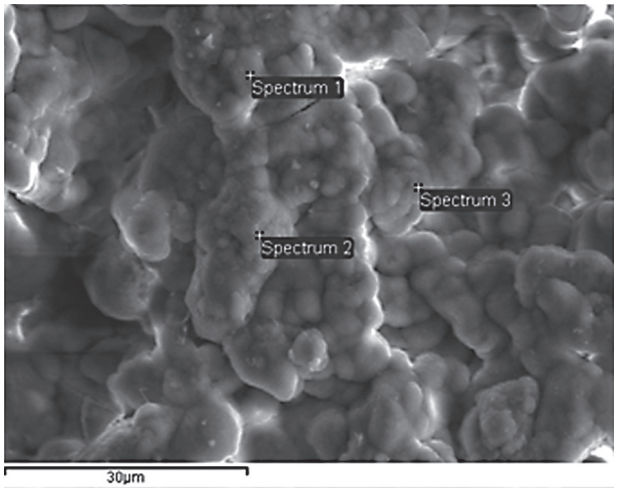

f) L4d (×2000)

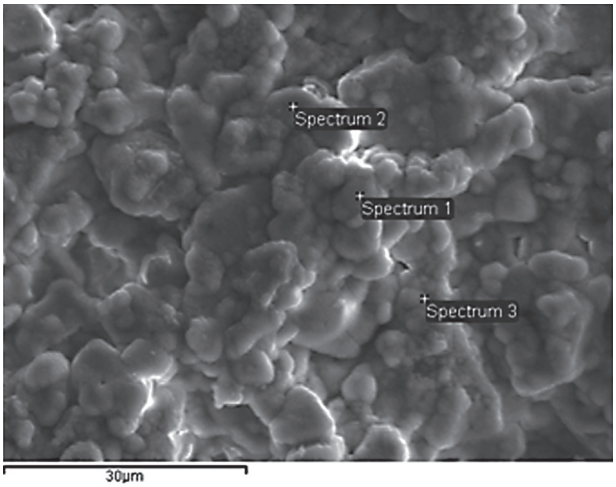

g) L4f (×500)

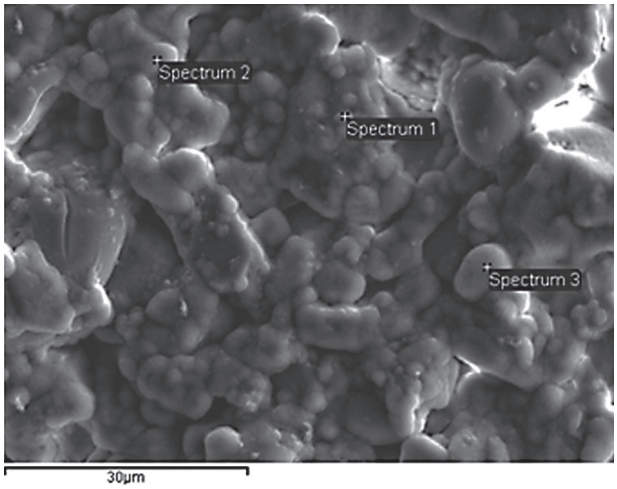

h) L4f (×2000)

Figure 4. SEM images of the laser treated part of the L1e (c, d), L4d (e, f), L4f (g, h) specimens after 6 days of immersion in DMEM solution. Magnification ×500 (c, e, g) and ×2000 (d, f, h).

of fluencies, led to the growth of a flake-like hydroxyapatite layer in the nano-scale within 3 days of immersion instead of 12, as it was shown in SEM and confirmed by TEM images. Such flake-like hydroxyapatite morphology might be explained by the non-photochemical effects caused by Nd:YAG laser, which may induce nucleation of amino acids in the solutions. Crystallization of glycine, L-alanine, L-histidine and L-glutamic acid,

that are abundant in DMEM solution, have been reported, under the irradiation of this kind of laser [13, 14]. The crystallized molecules of amino acids are supposed to play the role of matrices for hydroxyapatite deposition and, in this way, it might be possible to control crystal structure of hydroxyapatite during nucleation. The considerable impact of the laser application and the difference of the mechanism beyond hydroxyapatite precipitation via laser energy are enhanced by the fact that, under the same conditions of processing and bioactivity testing, only the Nd:YAG laser-treated half part of the specimen was covered with hydroxyapatite nano-film. The other untreated half part of the same specimen showed no sign of precipitation. On the other hand, as far as the Er:YAG application is concerned - which presents high optical absorption coefficient of water at the wavelength 2940 nm [18] - full coverage, of both the laser treated and untreated half parts of 4 specimens' surfaces with hydroxyapatite of typical features was observed [21], after 6 days of immersion in DMEM solution, almost the half time observed in the control specimens. The expansion of hydroxyapatite precipitation to the untreated side of the specimens may be attributed to the fact that the high-power Er:YAG laser radiation on a strongly absorbing liquid is related to intense surface evaporation, which results in the motion of the liquid under the reactive action of recoil vapors [22]. The formation of hydroxyapatite at both types of laser irradiated surfaces of the specimens, simultaneously immersed in DMEM, might be explained by formation of ablation plasma of the ejected material on the solid-liquid interface [5, 23]. Due to the laser induced pressure and the strong confinement effect of DMEM, the laser-induced plasma is driven to a high-temperature, high density and high-pressure state [5, 23]. These thermodynamic conditions are related to changes of Gibbs free energy and metastable Ca-P phase transformations inside the plasma plume [24, 25]. The plasma plume expands in the liquid, causing ejection of nano clusters from the material. Water molecules of the solution at the processing region are vaporized by the high energy of plasma and form cavitation bubble. In this way the concentration of various ions in the plasma increased greatly in a very short time, and great degree of super-saturation is obtained. These supersaturated ions would be more active and easily deposited [26]. Finally, a rapid quenching of plasma plume leads to nucleation of the calcium phosphate phases and growth of the nuclei on the materials surface [25]. Since the nano clusters of material surface are ejected during LLSI, causing changes in surface energy, the Ca-P particles immediately attach the defect sites. Concluding, despite the fact that the preliminary data of the present study seem to highlight the impact of laser application on the optimization of the bioactive behaviour developed by dental porcelain modified by bioactive glass, further investigation of the interaction mechanisms at the laser-liquid-material interface is required, so that the occurred drastic state can be properly tuned with laser parameters and to better tailor the bioactivity.

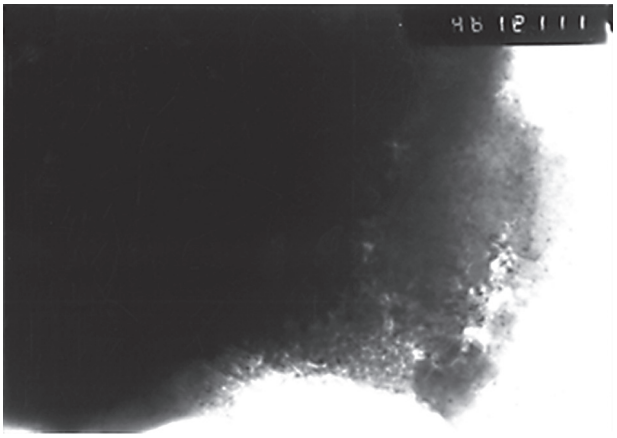

a) bright field electron micrograph

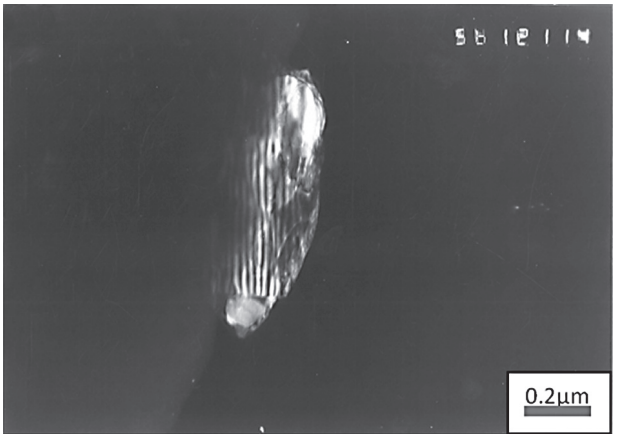

b) dark field electron micrograph

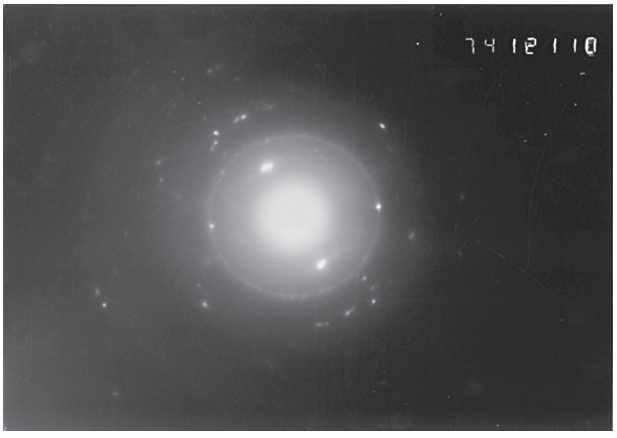

c) diffraction pattern corresponding to the area where the grain was detected.

Figure 5. TEM image of the laser treated part of the LN3b specimen after 3 days of immersion in DMEM solution: a) bright field electron micrograph, b) dark field electron micrograph, c) diffraction pattern corresponding to an area where the grain was detected.

CONCLUSIONS

Under the limitation of the present study it appears that the treatment of dental porcelain modified by bioactive glass composite material with Nd:YAG and Er:YAG laser energy under certain range of fluencies may accelerate the hydroxyapatite formation on their surfaces and improve their bioactive behaviour. Furthermore, treatment with Nd:YAG laser of specific parameters causes the precipitation of flake-like hydroxyapatite in the nano-scale. However, further research in estimation of mechanisms of LLSI is required in order to find out the optimal conditions for early and controlled hydroxyapatite precipitation.

Acknowledgement

One of the authors, A. Beketova, acknowledges the Erasmus Mundus BMU LOT7 Program for the financial support of this work.

References

1. Godouri O.M., Kontonasaki E., Chatzistaurou X., Papadopoulou L., Koidis P., Paraskevopoulos K.M.: Key Eng. Mater. *396-398*, 199 (2009).
2. Godouri O.M., Kontonasaki E., Kantiranis N., Chatzistaurou X., Papadopoulou L., Koidis P., Paraskevopoulos K.M.: Key Eng. Mater. *396-398*, 95 (2009).
3. Godouri O.M., Kontonasaki E., Theocharidou A., Kantiranis N., Chatzistaurou X., Koidis P., Paraskevopoulos K.M.: Biocer. Develop. Appl. *1*, 1 (2011).
4. Liu P., Cui H., Wang C.X., Yang G.W.: Phys. Chem. Chem. Phys. *12*, 3942 (2010).
5. Yang, G.W.: Progr. Mater. Sci. *52*, 648 (2007).
6. Pecheva E., Petrov T., Lungu C., Montgomery P., Pramatarova L.: Chem. Eng. J. *137*, 144 (2008).
7. Zhong J., Greenspan D.C.: J. Biomed. Mater. Res.: Appl. Biomater. *53*, 694 (2000).
8. Gibson I.R., Rehman I., Best S.M., Bonfield, W.: J. Mater. Sci.: Mater. Med. *11*, 799 (2000).
9. Stoch A., Jastrzebski W., Brozek A., Stoch J., Szaraniec J., Trybalska B., Kmita G.: J. Mol. Struct. *555*, 375 (2000).
10. Data from International Centre of Diffraction Data (ICDD) http://www.icdd.com
11. Georgiou S., Koubenakis, A.: Chem. Rev. *103*, 349 (2003).
12. Poondi D., Dobbins T., Singh, J.: J. Mater. Sci. *35*, 6237 (2000).
13. Pramatarova L., Pecheva E., Presker R., Pham M.T., Maintz M.F., Stutzman, M.: Eur. Cells Mater. *9*, 9 (2005).
14. Pramatarova L., Pecheva E., Presker R.: Plasma Process. Polym. *3*, 248 (2006).
15. Pramatarova L., Pecheva E., Dimova-Malinovska D., Pramatarova D., Bismayer U., Petrov T., Minkovsky N.: Vacuum, *76*, 135 (2004).
16. Goudouri O.M., Kontonasaki E., Theocharidou A., Kantiranis N, Chatzistaurou X, Koidis P., Paraskevopoulos K.M.: Matters Chem. Phys. *125*, 309 (2011).
17. Hench L.L., Wheeler D.L., Greenspan D.C.: J Sol-Gel Sci. Tech. *13*, 245 (1998).
18. Hale G.M., Querry M.R.: Appl. Optics. *12*, 555 (1973).
19. Garetz B.A., Matic J.: Phys. Rev. Lett. *89*, 1 (2002).
20. Sun X., Garetz B.A., Myerson A.S.: Cryst. Growth Design *8*, 1 (2008).
21. LeGeros R.Z.: Progr. Chrystal Growth Charact. *4*, 1 (1981).
22. Dolgaev S.I., Simakin A.V., Shafeev G.A.: Quantum Electronics *32*, 443 (2002).
23. Besner S., Meunier M. in: *Laser precision microfabrication*, p. 163-187, ed. Sugioka, K., Meunier, M., Pique, A., Springer-Verlag, Berlin (2010).
24. Hu S., Li W., Liu W., Dong Y., Cao S., Yang J.: J. Phys. Condens. Mater. *23*, 205302_1 (2011).
25. Liu P., Wang C., Chen J., Xu N., Yang, G.: J. Phys. Chem. C *113*, 12154 (2009).
26. Wang H., Liang C., Yang Y., Li, C.: Biomed. Mater. *5*, 1 (2010).